Electronic Supplementary Material (ESI) for Lab on a Chip.

Supporting Information

Dual-pore glass chips for cell-attached single-channel recordings

Brandon R. Bruhn[a] , Haiyan Liu[a], Stefan Schuhladen[a], Alan J. Hunt[a], Aghapi Mordovanaki[a,b] and Michael Mayer[a,c,1]

[a]Department of Biomedical Engineering, University of Michigan, Ann Arbor, MI 48109, USA
[b]Center for Ultrafast Optical Science, University of Michigan, Ann Arbor, MI 48109, USA
[c]Department of Chemical Engineering, University of Michigan, Ann Arbor, MI 48109, USA
[1]To whom correspondence should be addressed. e-mail: mimayer@umich.edu

Table of Contents

Section S1. Schematic of machining setup 2
Section S2. Measuring the ablation threshold 2
Section S3. Measuring tilt in the coverslip surface 3
Section S4. Estimating the resistance contribution and length of the single-shot aperture 3
Section S5. Characterizing the capacitance of the recording setup 4
Section S6. Characterizing noise in the presence of a gigaseal 5
Section S7. Cell-attached single-channel recordings of BK channels 6

Section S1. Schematic of machining setup

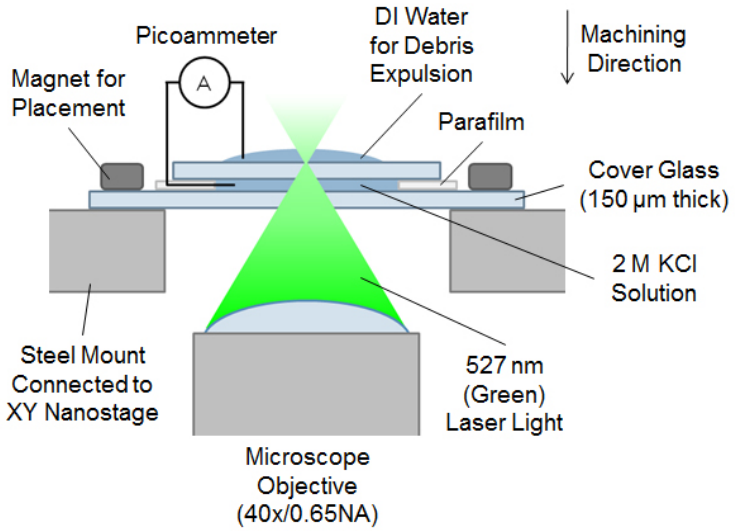

Fig. S1 Schematic representation of the machining setup used for femtosecond laser ablation of the recording and positioning pores (Fig. 2a-b). Since the laser passes through media with different indices of refraction, changes in the vertical position of the objective do not directly equal the corresponding changes in the position of the focal spot. For instance, we only need to move the objective by 92 µm in order for the focal spot to traverse the entire 150 µm thickness of a glass coverslip. As a result, we multiplied all vertical step sizes by a factor of 0.61 to determine how far to move the objective during machining.

Section S2. Measuring the ablation threshold

We measured single-shot and high-repetition-rate ablation thresholds at the beginning of each day of machining to account for drift in the laser profile and pulse width. Here, we define an ablation threshold as the lowest laser power that produces visible damage on the surface of the glass coverslip as viewed under brightfield microscopy. We used the same objective that focuses the laser into the substrate to observe the laser-induced damage. The procedure for measuring the ablation threshold is simple. First, we adjusted the position of the objective to bring the image of the glass surface into focus. Next, we attempted to ablate the surface as we varied the focal plane about the starting position; this was necessary to account for a slight difference between the position of the laser focus and the imaging plane. When measuring the single-shot threshold, we adjusted the lateral position of the laser focus between shots to avoid effects from sub-threshold modification to the glass. When measuring the high-repetition-rate threshold, we scanned the laser focus about a line at each focal plane. After attempting to ablate the surface at a particular power, we adjusted the power either up or down to find the threshold at which damage started to occur or no longer occurred. The ablation threshold was generally higher at the top surface of the glass in comparison to the bottom surface (see Fig. 2b), which is likely due to spherical aberration.

Section S3. Measuring tilt in the coverslip surface

When machining the L-shaped channels shown in Fig. 2c, we accounted for tilt in the coverslip to avoid cracking or incomplete ablation resulting from focusing the laser too far below the surface. At three separate non-collinear *x*-*y* coordinates, we determined the position of the uppermost focal plane that yielded visible single-shot damage in order to calculate the tilt (assuming a flat surface). Tilt was negligible when machining the positioning and recording pores (Fig. 2b) as they span a relatively small lateral distance.

Section S4. Estimating the resistance contribution and length of the single-shot aperture

The access resistance of a dual-pore chip can be described by the following equation:

$$R_A = R_L + R_P \quad \textbf{(1)}$$

where R_A is the access resistance, R_L is the resistance of the segment of the L-shaped channel that is upstream of the recording pore, and R_P is the resistance of the recording pore. Using Pouillet's law, we can derive an expression for R_L:

$$R_L = \frac{\rho L_L}{w_L h_L} \quad \textbf{(2)}$$

where ρ is the resistivity of the electrolyte solution, L_L is the channel length, w_L is the channel width, and h_L is the channel height. Assuming the single-shot aperture located at the entrance of the recording pore (Fig. 2a) is a perfect cylinder and neglecting access resistance, R_P can be described as follows:

$$R_P = \frac{4\rho h_C}{\pi D_1 D_2} + \frac{4\rho(t - h_C - L_{SS})}{\pi D_2^2} + \frac{4\rho L_{SS}}{\pi D_{SS}^2} \quad \textbf{(3)}$$

where h_C is the height of the conical segment of the pore (see Fig. 2b), D_1 is the pore diameter at the top surface of the coverslip, D_2 is the diameter at the bottom of the conical segment, t is the thickness of the coverslip, L_{SS} is the length of the single-shot aperture, and D_{SS} is the diameter of the single-shot aperture. The first term of this expression is the resistance of the conical segment of the pore, the second term is the resistance of the cylindrical segment of the pore, and the third term is the resistance of the single-shot aperture. Combining the above equations and solving for L_{SS} yields:

$$L_{SS} = \left[\frac{\pi D_2^2}{4}\left(\frac{R_A}{\rho} - \frac{L_L}{w_L h_L}\right) + h_C\left(1 - \frac{D_2}{D_1}\right) - t\right]\left(\frac{D_2^2}{D_{SS}^2} - 1\right)^{-1} \quad \textbf{(4)}$$

Assuming D_{SS} equals 250 nm, L_{SS} varies between 1 to 10 μm and is 5 ± 2 μm on average (N = 18 chips). Based on these estimates of length, the resistance of the aperture varies between 9 to 103 MΩ (37 to 89% of the access resistance) and is 49 ± 25 MΩ (78% of the access resistance) on average. Furthermore, the resistance of the remainder of the recording pore is 13 ± 1 MΩ and accounts for 10 to 60% of the access resistance. Finally, R_L is equal to 0.7 MΩ and accounts for less than 3% of the access resistance.

Section S5. Characterizing the capacitance of the recording setup

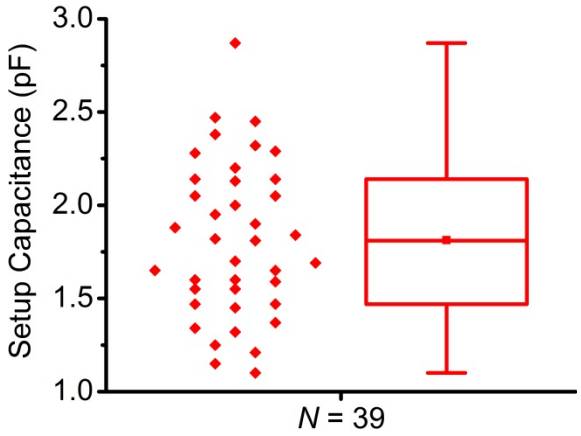

Fig. S2 Total capacitance of the recording setup. Each data point is from a different experiment. The raw data is shown on the left and a corresponding boxplot is shown on the right. The box encompasses the middle 50 percent of the data, the horizontal line and point inside the box show the median and mean values, respectively, and the whiskers extend to data points that are within 1.5 * IQR from the 25th and 75th percentiles. We obtained capacitance values by using the "Auto C-fast" function in the PatchMaster software to cancel the fast capacitive transients that occur upon the application of a voltage pulse.

Section S6. Characterizing noise in the presence of a gigaseal

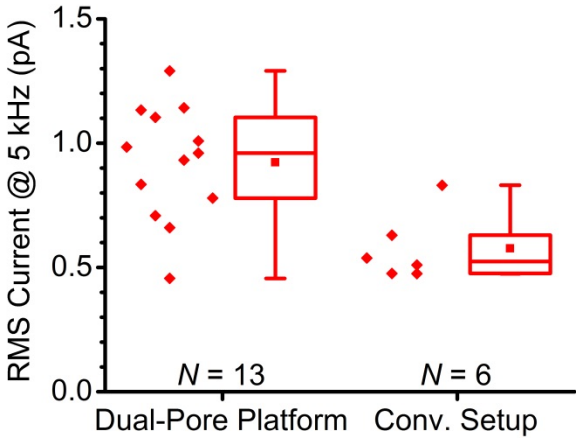

Fig. S3 RMS current measured after forming a gigaseal with both the dual-pore platform (left) and a conventional patch-clamp setup (right). Each data point shows the minimum RMS current measured in each experiment. The raw data is shown on the left and a corresponding boxplot is shown on the right. The box encompasses the middle 50 percent of the data, the horizontal line and point inside the box show the median and mean values, respectively, and the whiskers extend to data points that are within 1.5 * IQR from the 25th and 75th percentiles. We obtained all current traces at a bandwidth of 5 kHz and an applied potential of ±50 mV. We calculated each RMS current value using a region of the current trace in which no single-channel activity was present (*i.e.* when all ion channels were in the closed state or no channels were present in the patch).

Section S7. Cell-attached single-channel recordings of BK channels

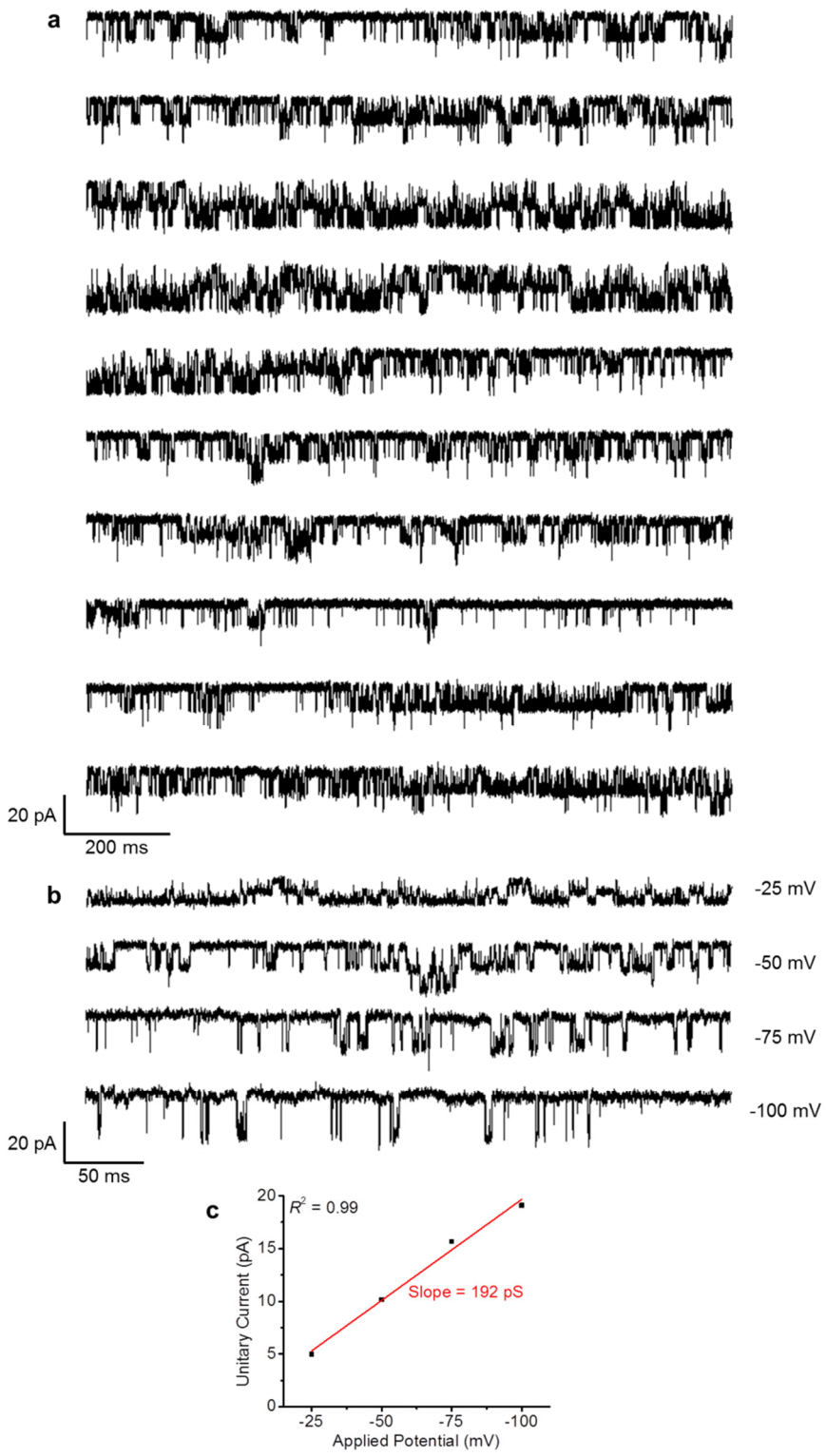

Fig. S4 Measuring the activity of single BK channels in the cell-attached configuration. (**a**) 12-s-long current trace obtained at a bandwidth of 5 kHz (as plotted) and an applied potential of -50 mV. (**b**) Current traces obtained at -25, -50, -75, and -100 mV. With increasing depolarization, the open-state probability of the BK channels increases, as expected. (**c**) Plot of the unitary (*i.e.* single-channel) current versus the applied potential. The red line is a best-fit. The slope of this line provides an estimate of the single-channel conductance, which agrees well with the value measured at -50 mV of 203 pS (6% difference) and falls within the range of previously published values (100 to 270 pS).